

**Electron-impact single ionization of Fe<sup>3+</sup> from the ground and metastable states**Aušra Kynienė<sup>✉</sup>,\* Sigitas Kučas, Saulius Pakalka, Šarūnas Masys, and Valdas Jonauskas<sup>✉</sup>*Institute of Theoretical Physics and Astronomy, Vilnius University, Saulėtekio Avenue 3, LT-10257 Vilnius, Lithuania*

(Received 27 June 2019; published 18 November 2019)

Single ionization by electron impact of the Fe<sup>3+</sup> ion is investigated using the Dirac-Fock-Slater approximation for the levels of the ground and first-excited 3d<sup>4</sup>4s configuration. Contributions from direct ionization (DI) and excitation-autoionization (EA) processes are taken into account. The scaled distorted-wave (DW) cross sections for DI and excitation by electron impact are used to analyze the experimental data. The study demonstrates the importance of correlation effects for the EA process. Good agreement with experimental data reveals that currently available DW cross sections and, therefore, the corresponding Maxwellian rate coefficients for electron-impact ionization process in Fe<sup>3+</sup> are overestimated and their usage may lead to wrong predictions for charge state distribution in plasma.

DOI: [10.1103/PhysRevA.100.052705](https://doi.org/10.1103/PhysRevA.100.052705)**I. INTRODUCTION**

Spectra from astrophysical objects such as the Sun, A- and B-type stars, interstellar material, and active galactic nuclei are rich in emission and absorption lines from various iron ions. The complex spectra from such astrophysical objects give important information about the structure and dynamics of their environments. Modeling of these spectral lines requires reliable atomic data. Electron-impact ionization and radiative recombination in addition to dielectronic recombination define charge state distribution in collisionally ionized plasma. Such plasmas are observed in astrophysical objects such as stellar coronal, supernova remnant, galaxies, and galaxy clusters. The structure of spectral lines is determined by the population of levels in the different ionization stages.

The aim of the current work is to study electron-impact ionization cross sections for the Fe<sup>3+</sup> ion. The electron-impact ionization process in Fe<sup>3+</sup> was previously investigated up to electron energies of 80 eV using the configuration average distorted-wave (CADW) approximation [1]. Their study included direct ionization (DI) and the 3p → 3d excitation for the indirect process. Calculations [2] that considered the direct process in addition to the 3p → 3d excitation with subsequent autoionization demonstrated quite good agreement with measurements at higher energies [3]. The experimental cross sections for the Fe<sup>3+</sup> ion were observed by employing the animated crossed-beams technique [4]. Unfortunately, other excitation-autoionization (EA) channels corresponding to excitations to the higher shells were not considered in these calculations [1,2]. Furthermore, it was noticed [3] that the onset in the data at ~35 eV indicates the presence of metastable ions in the ion beam. In addition, it was suggested that the excited levels of the ground configuration may also contribute to the measured cross sections. However, no study regarding a metastable fraction in the ion beam was presented.

Recent calculations for the ground configuration [5] using the CADW approximation provided overestimated data compared to the measurements [3]. These calculations included excitations from the 3s and 3p shells up to shells with the principal quantum number n = 12. The discrepancy of ~25% was obtained for the peak value. What is more, the previous level-to-level DW (LLDW) calculations [6] using the Dirac-Fock-Slater (DFS) approach demonstrated quite good agreement with the CADW data [1,2,5]. These works did not explain the discrepancies among the theoretical and experimental values.

Our study of the electron-impact ionization process in Fe<sup>3+</sup> includes the ground and the first-excited configurations. The scaled cross sections for the DI and excitation processes are studied to explain the measurements. In addition, the correlation effects are investigated for the DI and strongest excitations from the considered configurations.

The paper is organized as follows. In Sec. II, we describe the used methods to calculate cross sections and also present expressions for the scaled DW cross sections. In Sec. III, we compare our calculated results with the experimental values and provide Maxwellian rate coefficients for the levels of the ground and excited configurations.

**II. THEORETICAL APPROACH**

Energy levels, radiative and Auger transition probabilities, as well as electron-impact excitation and ionization cross sections are determined using the FLEXIBLE ATOMIC CODE (FAC) [7], which implements the DFS approach. The single-configuration approximation is used in this work. Therefore, the mixing of configuration state functions corresponding to the same configuration is taken into account. The study of electron-impact excitation and ionization cross sections is performed in the potential of the ionized ion.

Direct and indirect electron-impact ionization processes are investigated to obtain total electron-impact single-ionization cross sections. It is accepted to assume that the electron is removed from the atomic system instantly in the direct process. On the other hand, the EA process occurs

\*Ausra.Kyniene@tfai.vu.lt

when the atomic system is excited to an autoionizing state that decays to the next ionization stage through Auger transitions. Thus, the total electron-impact single-ionization cross section from level  $i$  of the  $\text{Fe}^{3+}$  ion to level  $f$  of the  $\text{Fe}^{4+}$  ion can be expressed by

$$\sigma_{if}(\varepsilon) = \sigma_{if}^{\text{DI}}(\varepsilon) + \sum_k \sigma_{ik}^{\text{EXC}}(\varepsilon) B_{kf}^a, \quad (1)$$

where  $\sigma_{if}^{\text{DI}}(\varepsilon)$  is the DI cross section at the incident electron energy  $\varepsilon$ , and  $\sigma_{ik}^{\text{EXC}}(\varepsilon)$  is the electron-impact excitation cross section to level  $k$  of the  $\text{Fe}^{3+}$  ion.

Autoionization branching ratio  $B_{kf}^a$  in the cross-section calculations leads to the radiative damping of the indirect process and is determined by the expression

$$B_{kf}^a = \frac{A_{kf}^a}{\sum_m A_{km}^a + \sum_n A_{kn}^r}, \quad (2)$$

where  $A^a$  and  $A^r$  are the Auger and radiative transition probabilities, respectively. Therefore, only contributions from the levels above the single-ionization threshold are taken into account. The summation over all final levels  $f$  of  $\text{Fe}^{4+}$  in Eq. (1) produces the total single-ionization cross sections for level  $i$ .

It is a well-known fact that the DW approximation often overestimates cross sections for neutral atoms or near-neutral ions. Therefore, the scaling factors were suggested to be used to diminish the DW cross sections for the electron-impact ionization and excitation processes [8]. The scaled cross sections for electron-impact excitation are expressed by the following equation [8,9]:

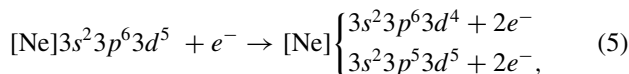
$$\sigma_{ik}^{\text{EXC}*}(\varepsilon) = \frac{\varepsilon}{\varepsilon + \Delta E_{ik} + \varepsilon_b} \sigma_{ik}^{\text{EXC}}(\varepsilon), \quad (3)$$

where  $\varepsilon_b$  is the binding energy of the electron and  $\Delta E_{ik}$  is a transition energy. The scaling for the DI cross sections is obtained using the following equation:

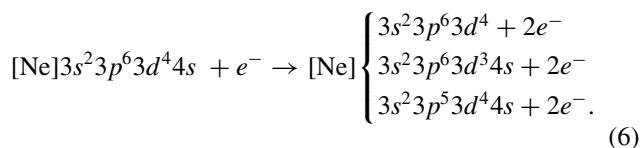
$$\sigma_{if}^{\text{DI}*}(\varepsilon) = \frac{\varepsilon}{\varepsilon + I} \sigma_{if}^{\text{DI}}(\varepsilon), \quad (4)$$

where  $I$  is the ionization energy.

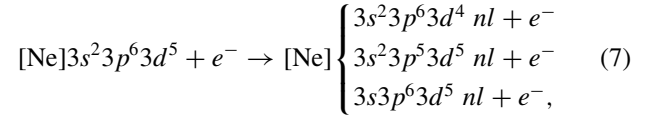
Ionization cross sections of the  $\text{Fe}^{3+}$  ion are investigated from the threshold up to 1000 eV. The ground configuration of the  $\text{Fe}^{3+}$  ion is  $[\text{Ne}] 3s^2 3p^6 3d^5$ . Here,  $[\text{Ne}]$  means a Ne-like electron structure, i.e., the orbitals of  $1s$ ,  $2s$ , and  $2p$  are fully occupied. The DI from the  $1s$ ,  $2s$ ,  $2p$ , and  $3s$  orbitals will result in the higher ionization stages rather than single ionization. Our study of the DI channels includes the ionization from the  $3p$  and  $3d$  shells of the ground configuration,



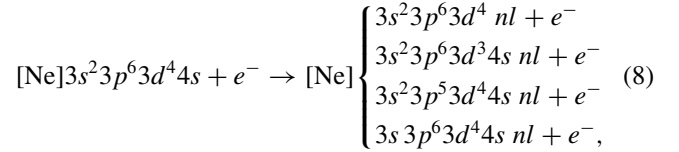
and for the first-excited configuration from the  $3p$ ,  $3d$ , and  $4s$  shells,



The EA process includes excitations from the  $3s$ ,  $3p$ , and  $3d$  shells of the ground configuration. These excitations are schematically shown as



where  $n \leq 8$  and  $l \leq 6$ . For the ground configuration, the 89 excited configurations are produced for which radiative and Auger decay processes are investigated. It should be noted that not all generated configurations are autoionizing. The excitations for the first-excited configuration are



where  $n \leq 8$  and  $l \leq 6$ . The 118 excited configurations are produced for the  $3d^4 4s$  configuration in the current study. It should be noted that the excitations to the higher shells ( $n > 8$ ) are not studied here since calculations for subconfigurations show that their contribution to the ionization process is negligible.

The influence of correlation effects is investigated for the direct ionization and strongest excitations from levels of the ground and  $3d^4 4s$  configurations. A list of admixed configurations having the largest influence to the considered configuration is generated by using configuration interaction strength (CIS). The CIS was defined previously by the equation [10–12]

$$T(K, K') = \frac{\sum_{\gamma\gamma'} \langle \Phi(K\gamma) | H | \Phi(K'\gamma') \rangle^2}{\bar{E}(K, K')^2}. \quad (9)$$

The summation in Eq. (9) is performed over all states  $\gamma$  and  $\gamma'$  of the  $K$  and  $K'$  configurations, respectively. The term  $\langle \Phi(K\gamma) | H | \Phi(K'\gamma') \rangle$  is the interconfiguration matrix element and  $\bar{E}(K, K')$  is an average energy distance between the configurations:

$$\begin{aligned} \bar{E}(K, K') &= \frac{\sum_{\gamma\gamma'} [\langle \Phi(K\gamma) | H | \Phi(K\gamma) \rangle - \langle \Phi(K'\gamma') | H | \Phi(K'\gamma') \rangle]}{\sum_{\gamma\gamma'} \langle \Phi(K\gamma) | H | \Phi(K'\gamma') \rangle^2} \\ &\times \langle \Phi(K\gamma) | H | \Phi(K'\gamma') \rangle^2. \end{aligned} \quad (10)$$

The CIS value [Eq. (9)] divided by statistical weight  $g(K)$  of the studied configuration  $K$  corresponds to the average contribution of the admixed configuration  $K'$  in the expansion of a wave function for  $K$ . The list of admixed configurations is built by considering single and double excitations from the shells with the principal quantum number  $n \geq 3$  up to shells with  $n = 8$ . The pseudorelativistic method [13] is used to obtain radial orbitals for the studied configurations. The same approach was previously used to study energy levels [14], electric [15] and magnetic [16,17] dipole transitions, Auger cascades [18–20], and electron-impact ionization cross sections [21–24].

The Maxwellian rate coefficients are obtained from the calculated cross sections for the electron-impact ionization

process in the  $\text{Fe}^{3+}$  ion. The rate coefficient  $\alpha_{ij}(T_e)$  for the Maxwellian-Boltzmann electron energy distribution at electron temperature  $T_e$  is given by

$$\alpha_{ij}(T_e) = \left(\frac{1}{k_B T_e}\right)^{\frac{3}{2}} \left(\frac{8}{m_e \pi}\right)^{\frac{1}{2}} \int_0^\infty \varepsilon \sigma_{ij}(\varepsilon) \exp\left(-\frac{\varepsilon}{k_B T_e}\right) d\varepsilon. \quad (11)$$

Here,  $k_B$  is the Boltzmann constant,  $m_e$  is the electron mass, and  $\sigma_{ij}(\varepsilon)$  is the cross section for the transition from level  $i$  to level  $j$ .

### III. RESULTS

The ground  $[\text{Ne}] 3s^2 3p^6 3d^5$  configuration has 37 energy levels, while the first-excited  $[\text{Ne}] 3s^2 3p^6 3d^4 4s$  configuration corresponds to 62 energy levels (Table I). The energy levels of the ground configuration calculated in the single-configuration approximation span the range of 14.69 eV, while the energy interval of 15.86 eV is occupied by the first-excited configuration. The widths of energy levels provided by the National Institute of Standards and Technology (NIST) [25] correspond to 13.42 and 11.79 eV for the ground and first-excited configurations, respectively. The obtained differences among our and NIST values can be explained by correlation effects which are not considered in this case. The lowest level of the  $3d^4 4s$  configuration is above the ground level by 14.61 eV. What is more, the single-ionization threshold is equal to 52.78 eV. The NIST recommended value for the single ionization equals  $54.91 \pm 0.04$  eV, which is slightly above our value. The same tendency for single-ionization thresholds obtained using FAC was noticed for other ions:  $\text{Se}^{2+}$  [22],  $\text{Se}^{3+}$  [21,23],  $\text{W}^{25+}$  [26],  $\text{W}^{26+}$  [27,28], and  $\text{W}^{27+}$  [29].

The energy levels and their lifetimes for the ground and first-excited configurations are shown in Table I. The probabilities of electric quadrupole and magnetic dipole transitions are calculated from these levels to determine the lifetimes. All these levels have lifetimes exceeding  $10^{-5}$  s—the amount of time that ions need to reach the interaction region with electrons [30].

There are many configurations that have energy levels that straddle the ionization threshold (Fig. 1). All of them correspond to excitations from the outer shell of the ground and first-excited configuration. The cross sections obtained from the lowest and highest levels of the ground configuration are compared to measurements in Fig. 2. The theoretical values overestimate the experimental data at the peak of the cross sections. The overestimated values are also obtained for the highest level of the ground configuration at the lower energies of the impacting electron. The cross sections produced by ionization from the ground level are below the measurements in the vicinity of the single-ionization threshold. As it was noticed before [3], the onset of the experimental cross sections at  $\sim 35$  eV indicates the presence of metastable ions in the ion beam. Interesting, the theoretical cross sections are within the error bars for the higher energies of the electron.

Theoretical cross sections calculated for the lowest and highest levels of the  $3d^4 4s$  configuration are compared to measurements in Fig. 3. All theoretical data are above the

experimental values. The largest difference is obtained for the lower energies of the impacting electron. A similar situation was also obtained for the single-ionization cross section of neutral carbon and  $\text{C}^{1+}$  ion [8]. It was suggested that other physical mechanisms appear on the scene for the ionization process in these charge states.

The contributions of the direct and indirect processes for the ground level and the lowest level of the  $3d^4 4s$  configuration are shown in Fig. 4. The EA channels corresponding to excitations up to shells with the principal quantum number  $n = 8$  are considered in the study since the excitations to the higher shells give negligible contribution. The direct process produces a slightly higher contribution for the ground level compared to the lowest level of the  $3d^4 4s$  configuration. This can be explained by the smaller number of electrons in the  $3d$  shell of the  $3d^4 4s$  configuration compared to the ground configuration. The DI cross sections for the  $4s$  shell do not compensate for the smaller number of electrons in the  $3d$  shell of the first-excited configuration. The EA cross sections for the  $3d^4 4s$  configuration are higher than for the ground configuration since excitations from the  $3d$  shell of the first-excited configuration produce autoionizing states which decay to  $\text{Fe}^{4+}$ . The  $3d$  shell is the outermost one for the ground configuration and, therefore, only a small contribution is provided to the EA process. For both configurations, the EA channels corresponding to excitations from the  $3p$  shell dominate starting from  $\sim 100$  eV.

The strongest EA channels for the ground level are shown in Fig. 5. The  $3p \rightarrow 3d$  excitation produces  $\sim 70\%$  of the total EA cross sections. The second highest cross section corresponds to the  $3p \rightarrow 4p$  excitation, which leads to the same parity configuration as the ground one.

A more complex situation regarding the strongest EA channels is obtained for the  $3d^4 4s$  configuration (Fig. 6). The  $3p \rightarrow 3d$  excitation dominates over the other channels as in the case of the ground configuration (Fig. 5). However, the excitations from the  $3d$  shell produce the strongest contribution at the lower energies of the electron. As it was mentioned above, the excitations from the  $3d$  shell produce small contribution to the EA cross sections for the ground configuration. The  $3d \rightarrow 4d$ ,  $3d \rightarrow 5d$ , and  $3p \rightarrow 4p$  excitations out of the five strongest EA channels lead to the same parity configurations as the initial one.

Previously, the scaled plane-wave Born (PWB) cross sections for electron-impact excitation were used to mimic the effects related to the polarizability of the atomic system [9]. Moreover, it was suggested that electron exchange, distortion, and polarization effects that are missing in the first-order PWB approximation are included in the calculations using the scaling functions. The studies of the electron-impact ionization process for neutral atoms and near-neutral ions using binary-encounter-dipole (BED) or binary-encounter-Bethe (BEB) models [31] with the scaled PWB cross sections [9] demonstrated a good agreement with the experimental data [9,32–34]. Recently, it was shown that the scaled DW cross sections can be used to explain the experimental data for neutral carbon and  $\text{C}^+$  ion [8]. Therefore, the same approach is applied here for the DW cross sections corresponding to ionization from the ground and first-excited configurations. The scaled DW cross sections for the lowest and excited levels

TABLE I. Lifetimes of the energy levels of the  $\text{Fe}^{3+} 3p^6 4d^5$  and  $3p^6 4d^4 4s$  configurations. Closed inner subshells are omitted in the notations of the levels. The levels are identified by the largest weight in the expansion of the wave function. Energies are given relative to the ground level energy.  $J$  is the total angular momentum quantum number. Note that  $a \pm b = a \times 10^{\pm b}$ .

Configuration	Index	Level	$J$	Energy (eV)	Lifetime (s)
$3p^6 4d^5$	0	$3d^2_-(2)3d^3_+(9/2)$	5/2	0.000	$\infty$
	1	$3d^2_-(2)3d^3_+(9/2)$	11/2	4.202	$\infty$
	2	$3d^2_-(2)3d^3_+(3/2)$	5/2	4.205	1.849+5
	3	$3d^2_-(2)3d^3_+(9/2)$	9/2	4.206	5.714+6
	4	$3d^2_-(2)3d^3_+(9/2)$	7/2	4.207	7.901+6
	5	$3d_+(5/2)$	5/2	4.834	5.517-1
	6	$3d^2_-(2)3d^3_+(5/2)$	3/2	4.844	8.460-1
	7	$3d^2_-(2)3d^3_+(5/2)$	1/2	4.856	6.533+3
	8	$3d^2_-(2)3d^3_+(9/2)$	7/2	5.248	1.920+1
	9	$3d^2_-(2)3d^3_+(3/2)$	1/2	5.262	8.743+0
	10	$3d_-(3/2)3d^4_+(2)$	3/2	5.269	8.284+0
	11	$3d_-(3/2)3d^4_+(2)$	5/2	5.271	7.709+0
	12	$3d^2_-(2)3d^3_+(9/2)$	11/2	5.980	1.372+2
	13	$3d^2_-(2)3d^3_+(9/2)$	13/2	5.983	4.373+3
	14	$3d_+(5/2)$	5/2	6.724	7.919-1
	15	$3d^2_-(2)3d^3_+(3/2)$	3/2	6.806	1.812+0
	16	$3d^2_-(2)3d^3_+(5/2)$	7/2	6.941	9.821-1
	17	$3d^2_-(2)3d^3_+(5/2)$	5/2	7.042	9.014-1
	18	$3d^2_-(0)3d^3_+(9/2)$	9/2	7.076	8.056-1
	19	$3d_-(3/2)3d^4_+(4)$	7/2	7.084	8.331-1
	20	$3d^2_-(2)3d^3_+(5/2)$	3/2	7.106	7.323-1
	21	$3d^5_+(5/2)$	5/2	7.109	6.846-1
	22	$3d^2_-(2)3d^3_+(5/2)$	9/2	7.361	1.591+0
	23	$3d_-(3/2)3d^4_+(4)$	11/2	7.392	7.797-1
	24	$3d^2_-(2)3d^3_+(3/2)$	7/2	7.632	8.911+0
	25	$3d_-(3/2)3d^4_+(4)$	9/2	7.664	4.628+0
	26	$3d^2_-(2)3d^3_+(3/2)$	5/2	8.229	3.273+0
	27	$3d^2_-(2)3d^3_+(3/2)$	7/2	8.229	3.234+0
	28	$3d^3_-(3/2)3d^2_+(2)$	1/2	9.121	8.949-1
	29	$3d^2_-(0)3d^3_+(3/2)$	3/2	10.067	4.713-1
	30	$3d^2_-(2)3d^3_+(5/2)$	5/2	10.067	3.778-1
	31	$3d^2_-(2)3d^3_+(5/2)$	7/2	11.097	5.783-2
	32	$3d^2_-(0)3d^3_+(9/2)$	9/2	11.099	5.866-2
	33	$3d^2_-(2)3d^3_+(5/2)$	1/2	13.626	1.930-2
	34	$3d^2_-(0)3d^3_+(3/2)$	3/2	13.626	1.946-2
	35	$3d_-(3/2)3d^4_+(0)$	3/2	14.689	2.186-2
36	$3d^2_-(0)3d^3_+(5/2)$	5/2	14.694	2.191-2	
$3p^6 3d^4 4s$	37	$3d^2_-(2)3d^2_+(2)4s_+(1/2)$	1/2	14.648	5.247-4
	38	$3d^3_-(3/2)3d_+(5/2)4s_+(1/2)$	3/2	14.675	5.209-4
	39	$3d^2_-(2)3d^2_+(4)4s_+(1/2)$	5/2	14.716	5.157-4
	40	$3d^2_-(2)3d^2_+(4)4s_+(1/2)$	7/2	14.765	5.099-4
	41	$3d_-(3/2)3d^3_+(9/2)4s_+(1/2)$	9/2	14.816	5.043-4
	42	$3d^3_-(3/2)3d_+(5/2)4s_+(1/2)$	1/2	16.502	3.024-4
	43	$3d^2_-(2)3d^2_+(4)4s_+(1/2)$	3/2	16.544	3.004-4
	44	$3d^2_-(2)3d^2_+(4)4s_+(1/2)$	5/2	16.601	2.979-4

TABLE I. (Continued).

Configuration	Index	Level	$J$	Energy (eV)	Lifetime (s)
	45	$3d_-(3/2)3d_+^3(9/2)4s_+(1/2)$	7/2	16.663	2.957-4
	46	$3d_+^3(3/2)3d_+(5/2)4s_+(1/2)$	7/2	17.846	4.565-4
	47	$3d_-^2(2)3d_+^2(4)4s_+(1/2)$	9/2	17.870	4.525-4
	48	$3d_-^2(2)3d_+^2(4)4s_+(1/2)$	11/2	17.899	4.483-4
	49	$3d_-(3/2)3d_+^3(9/2)4s_+(1/2)$	13/2	17.926	4.441-4
	50	$4s_+(1/2)$	1/2	18.021	4.655-4
	51	$3d_+^3(3/2)3d_+(5/2)4s_+(1/2)$	3/2	18.154	4.552-4
	52	$3d_-^2(2)3d_+^2(2)4s_+(1/2)$	3/2	18.289	3.865-4
	53	$3d_-^2(2)3d_+^2(2)4s_+(1/2)$	5/2	18.293	3.871-4
	54	$3d_-^2(2)3d_+^2(2)4s_+(1/2)$	7/2	18.301	3.835-4
	55	$3d_+^3(3/2)3d_+(5/2)4s_+(1/2)$	9/2	18.304	3.806-4
	56	$3d_+^4(2)4s_+(1/2)$	5/2	18.316	4.466-4
	57	$3d_-^2(2)3d_+^2(2)4s_+(1/2)$	5/2	18.603	3.984-4
	58	$3d_-^2(2)3d_+^2(2)4s_+(1/2)$	7/2	18.635	3.954-4
	59	$3d_-(3/2)3d_+^3(9/2)4s_+(1/2)$	9/2	18.662	3.924-4
	60	$3d_-(3/2)3d_+^3(9/2)4s_+(1/2)$	11/2	18.686	3.887-4
	61	$3d_-^2(2)3d_+^2(4)4s_+(1/2)$	9/2	18.972	2.643-4
	62	$3d_-^2(2)3d_+^2(4)4s_+(1/2)$	11/2	19.032	2.637-4
	63	$3d_+^3(3/2)3d_+(5/2)4s_+(1/2)$	1/2	19.186	2.748-4
	64	$3d_-(3/2)3d_+^3(5/2)4s_+(1/2)$	3/2	19.398	2.702-4
	65	$3d_+^3(3/2)3d_+(5/2)4s_+(1/2)$	7/2	19.402	2.959-4
	66	$3d_-^2(2)3d_+^2(2)4s_+(1/2)$	5/2	19.414	2.988-4
	67	$3d_-^2(2)3d_+^2(4)4s_+(1/2)$	13/2	19.658	3.314-4
	68	$3d_-(3/2)3d_+^3(9/2)4s_+(1/2)$	11/2	19.667	3.345-4
	69	$3d_-(3/2)3d_+^3(9/2)4s_+(1/2)$	7/2	19.673	2.597-4
	70	$3d_+^3(3/2)3d_+(5/2)4s_+(1/2)$	5/2	19.679	2.602-4
	71	$3d_-^2(2)3d_+^2(2)4s_+(1/2)$	3/2	19.699	2.593-4
	72	$3d_-(3/2)3d_+^3(3/2)4s_+(1/2)$	1/2	19.717	2.579-4
	73	$3d_-^2(2)3d_+^2(2)4s_+(1/2)$	7/2	19.733	2.597-4
	74	$3d_-(3/2)3d_+^3(9/2)4s_+(1/2)$	9/2	19.788	2.278-4
	75	$3d_+^4(4)4s_+(1/2)$	9/2	19.899	3.657-4
	76	$3d_+^4(4)4s_+(1/2)$	7/2	19.913	3.234-4
	77	$3d_-(3/2)3d_+^3(3/2)4s_+(1/2)$	1/2	20.630	2.962-4
	78	$3d_-(3/2)3d_+^3(9/2)4s_+(1/2)$	5/2	20.779	2.523-4
	79	$3d_-(3/2)3d_+^3(3/2)4s_+(1/2)$	3/2	20.794	3.223-4
	80	$3d_+^4(2)4s_+(1/2)$	5/2	21.008	3.178-4
	81	$3d_+^4(2)4s_+(1/2)$	3/2	21.018	2.510-4
	82	$3d_-(3/2)3d_+^3(3/2)4s_+(1/2)$	7/2	21.882	2.395-4
	83	$3d_-(3/2)3d_+^3(3/2)4s_+(1/2)$	5/2	21.888	2.502-4
	84	$3d_-^2(0)3d_+^2(4)4s_+(1/2)$	9/2	22.691	1.577-4
	85	$3d_-^2(2)3d_+^2(0)4s_+(1/2)$	3/2	22.698	1.588-4
	86	$3d_-(3/2)3d_+^3(5/2)4s_+(1/2)$	7/2	22.701	1.587-4
	87	$3d_-(3/2)3d_+^3(5/2)4s_+(1/2)$	5/2	22.701	1.589-4
	88	$3d_-^2(0)3d_+^2(2)4s_+(1/2)$	5/2	22.731	1.403-4
	89	$3d_-(3/2)3d_+^3(5/2)4s_+(1/2)$	3/2	22.838	1.398-4
	90	$3d_+^4(0)4s_+(1/2)$	1/2	22.891	1.401-4

TABLE I. (Continued).

Configuration	Index	Level	$J$	Energy (eV)	Lifetime (s)
	91	$3d^2_-(0)3d^2_+(4)4s_+(1/2)$	7/2	23.800	1.693–4
	92	$3d^2_-(2)3d^2_+(0)4s_+(1/2)$	5/2	23.808	1.657–4
	93	$3d^2_-(0)3d^2_+(2)4s_+(1/2)$	3/2	23.867	1.843–4
	94	$3d_-(3/2)3d^3_+(5/2)4s_+(1/2)$	1/2	23.988	1.844–4
	95	$3d_-(3/2)3d^3_+(5/2)4s_+(1/2)$	9/2	24.049	1.614–4
	96	$3d_-(3/2)3d^3_+(5/2)4s_+(1/2)$	7/2	24.058	1.606–4
	97	$3d^2_-(0)3d^2_+(2)4s_+(1/2)$	5/2	27.098	1.234–4
	98	$3d^2_-(0)3d^2_+(2)4s_+(1/2)$	3/2	27.099	1.232–4
	99	$3d^2_-(0)3d^2_+(0)4s_+(1/2)$	1/2	30.504	9.564–5

of the ground configuration are shown in Fig. 7. In addition, the single-configuration DW data along the measurements are presented for comparison. The largest effect of scaling is obtained for the lower energies of the impacting electron. It can be seen that all theoretical data for the ground level are below the experimental errors. On the other hand, the highest level of the ground configuration demonstrates good agreement with measurements for the higher energies. However, these cross sections are below the error bars for the lower electron energies, except in the region from 40 to 50 eV where the theoretical values are slightly above the measurements.

The scaled DW cross sections for the lowest and highest levels of the first-excited  $3d^44s$  configuration are shown in Fig. 8. Single-configuration DW cross sections and experimental values are presented for comparison. The cross sections for the lowest level of the configuration are in quite good agreement with the measurements for electron energies starting from 60 eV. On the other hand, the theoretical cross sections are above experimental error bars in the 40–60 eV

region. The theoretical cross sections obtained for the highest level of the configuration overestimate the measurements.

The underestimated scaled DW cross sections with respect to the measurements for the levels of the ground configuration (Fig. 6) suggest that the levels of the excited  $3d^44s$  configuration are present in the ion beam. Nevertheless, the theoretical values for the levels of the  $3d^44s$  configuration are above the error bars in the range of 40–60 eV. This demonstrates that some additional effects have to be considered to explain the observed data. Therefore, the influence of correlation effects is analyzed for the direct ionization and strongest excitations from the levels of the ground and  $3d^44s$  configurations. It should be noted that the correlation effects have a small effect on the cross sections of the direct process. However, a different situation is observed for EA. The study included the  $3p \rightarrow 3d$  and  $3p \rightarrow 4p$  excitations for the ground configuration and  $3p \rightarrow 3d$ ,  $3d \rightarrow 4d$ ,  $3d \rightarrow 5d$ , and  $3p \rightarrow 4p$  for the  $3d^44s$  configuration. The bases of interacting configurations are generated using the CIS values [Eq. (9)] for the autoionizing configurations. However, only a negligible influence of the correlation effects to the EA cross sections is found for the ground configuration, even though the correlation effects

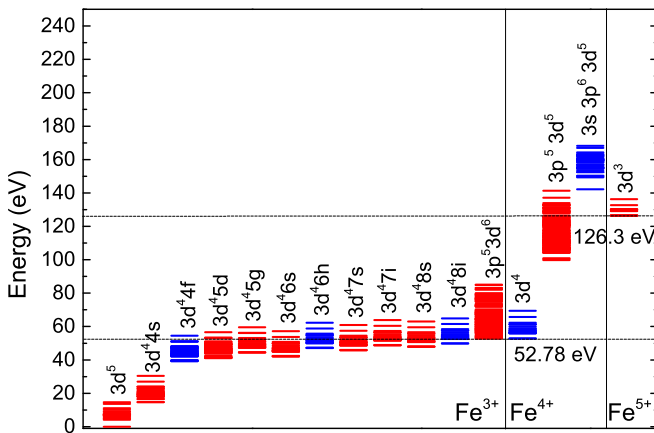


FIG. 1. Energy levels of the ground configurations for the  $\text{Fe}^{3+}$ ,  $\text{Fe}^{4+}$ ,  $\text{Fe}^{5+}$  ions in addition to energy levels that straddle the single-ionization threshold. The first-excited configuration of  $\text{Fe}^{3+}$  as well as  $3p^53d^5$  and  $3s3d^5$  of  $\text{Fe}^{4+}$  are also presented. For the  $\text{Fe}^{3+} 3d^4nl$  ( $n = 5-8$ ) configurations, only the configurations with the lowest orbital quantum number  $l$  and the largest one are shown. Red (light): even configurations; blue (dark): odd configurations.

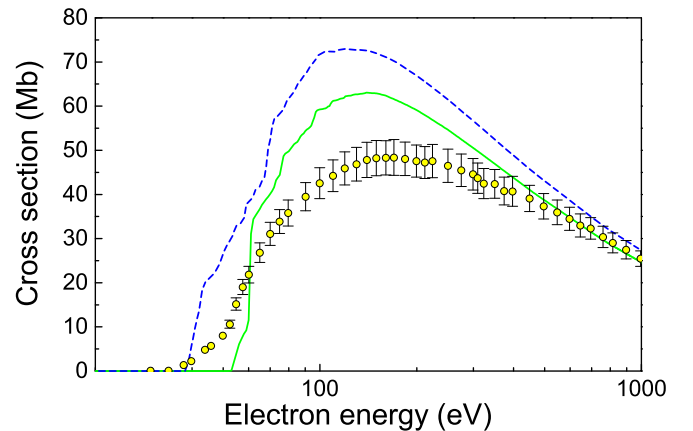


FIG. 2. Single-ionization cross sections for the ground configuration levels: solid green line corresponds to the level with index 0 (Table I); dashed blue line corresponds to level 36. Experiment: open circles with error bars [3]. Logarithmic scale is used for electron energies.

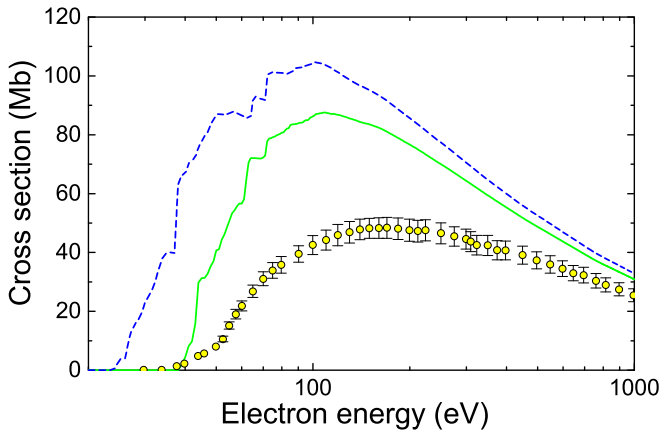


FIG. 3. Single-ionization cross sections for the ground configuration levels: solid green line corresponds to level with index 37 (Table I); dashed blue line corresponds to level 99. Experiment: open circles with error bars [3]. Logarithmic scale is used for electron energies.

diminish the scaled cross sections by approximately 20% for the levels of the first-excited configuration (Fig. 9). Thus, the difference of  $\sim 50\%$  is obtained among the cross sections calculated without scaling and ones with scaling along the correlation effects. The correlation effects for the scaled cross sections of the lowest level of the excited configuration lead to values below the measurements from the threshold energy up to 200 eV and within the error bars for the higher energies. On the other hand, the cross sections for the highest level of the  $3d^4 4s$  configuration are above measurements from the threshold energy up to 70 eV and starting from  $\sim 200$  eV.

The comparison with measurements for the level with index 67 is presented in Fig. 10. This level together with level 49 (Table I) have the largest values of the total angular momentum quantum number  $J$  for the  $3d^4 4s$  configuration. The levels with the largest statistical weights would be populated

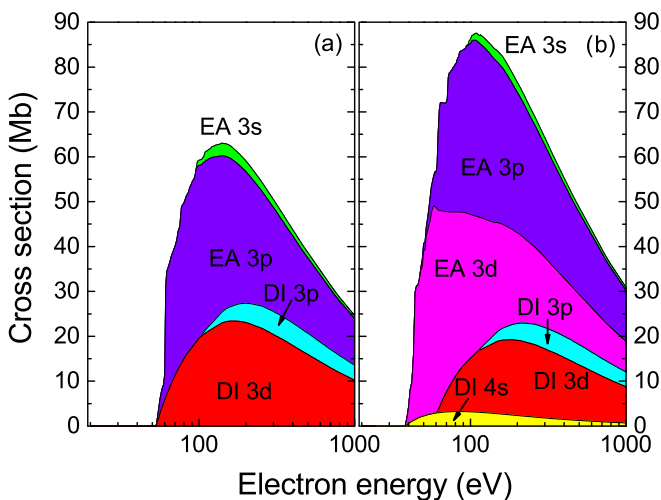


FIG. 4. Comparison of contribution from the DI and EA channels for the single ionization of  $\text{Fe}^{3+}$ : (a) ground configuration and (b) the lowest level of the  $3d^4 4s$  configuration. Logarithmic scale is used for electron energies.

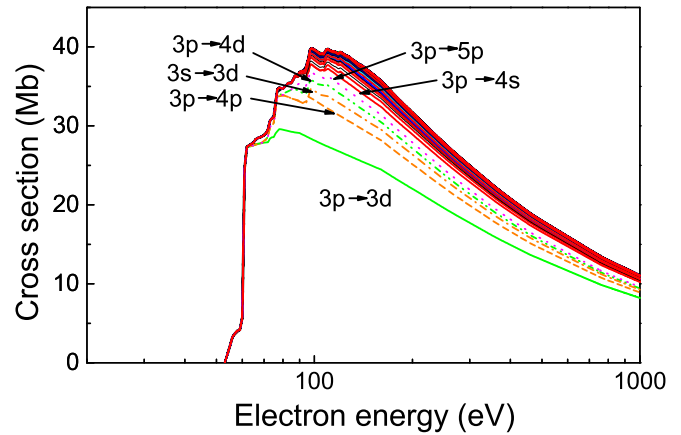


FIG. 5. Accumulated cross sections of the EA channels contributing to the ionization of the ground level of  $\text{Fe}^{3+}$ . The strongest EA contributions are individually identified. Logarithmic scale is used for electron energies.

with the largest probability in the ion beam. On the other hand, the Boltzmann distribution or even collisional radiative modeling with subsequent radiative cascade may have to be used to determine the population of the levels. However, these modelings would require a separate study. One can see that the theoretical cross sections are still below the experimental values in the energy range from approximately 50 to 150 eV. This difference can be explained by the resonant excitation double-autoionization process, which is not investigated in this work.

What is more, the study of the electron-impact single ionization for the  $\text{Se}^{2+}$  [22] and  $\text{Se}^{3+}$  [23] ions demonstrated that direct double ionization has a diminishing effect on the theoretical single-ionization cross sections if it is assumed that the multistep processes determine the direct double ionization by electron impact [35,36]. The calculated direct double-ionization cross sections have a value of  $\sim 1$  Mb at the peak [5]. Therefore, the single-configuration cross sections for  $\text{Fe}^{3+}$  would be diminished by approximately 1 Mb starting from the double-ionization threshold (126 eV).

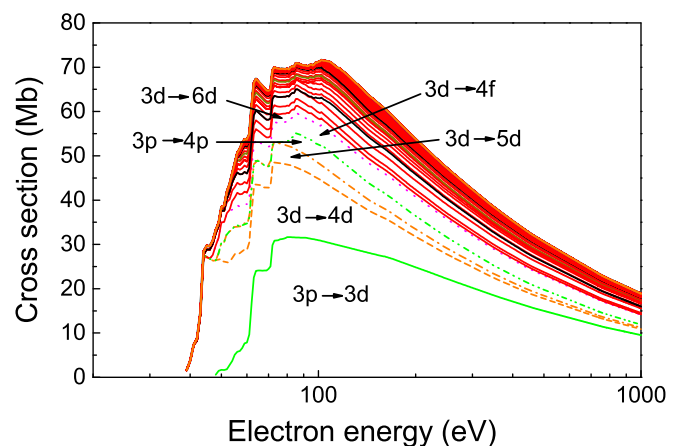


FIG. 6. The same as Fig. 5, but for the lowest level of the  $3d^4 4s$  configuration.

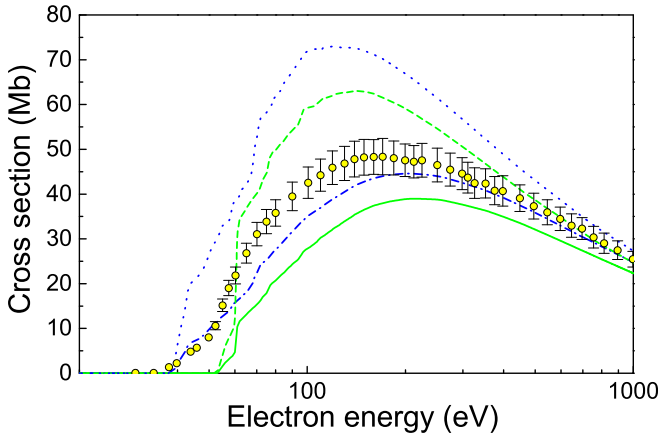


FIG. 7. Single-ionization cross sections obtained with and without the scaling functions [Eqs. (3) and (4)] for the levels of the ground configuration. Solid green line: scaled DW cross sections for level with index 0 (Table I); dashed green line: DW cross sections for level 0; dash-dotted blue line: scaled DW cross sections for level 36; dotted blue line: DW cross sections for level 36. Experiment: open circles with error bars [3]. Logarithmic scale is used for electron energies.

Finally, the obtained good agreement with the experimental data for the scaled cross sections that include correlation effects shows that the currently available DW data for electron-impact single ionization in  $\text{Fe}^{3+}$  are overestimated compared to measurements and, therefore, their usage may lead to wrong conclusions about a charge state distribution in plasma. The Maxwellian rate coefficients for the lowest and highest levels of the ground and excited  $3d^44s$  configurations in addition to level 67 (Table I) are presented in Table II.

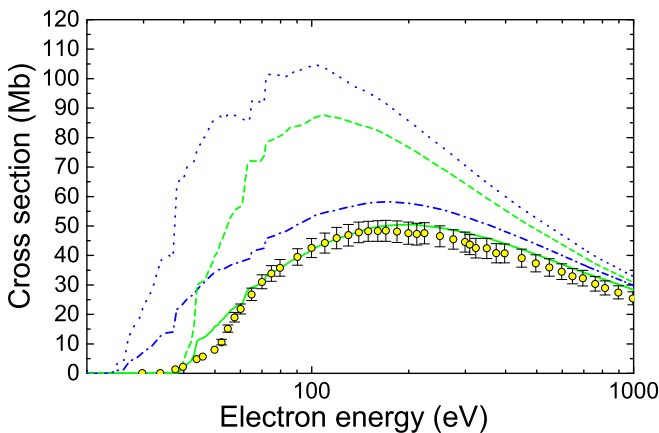


FIG. 8. Single-ionization cross sections obtained without and with the scaling functions [Eqs. (3) and (4)] for the levels of the  $3d^44s$  configuration. Solid green line: scaled DW cross sections for level with index 37 (Table I); dashed green line: DW cross sections for level 37; dash-dotted blue line: scaled DW cross sections for level 99; dotted blue line: DW cross sections for level 99. Experiment: open circles with error bars [3]. Logarithmic scale is used for electron energies.

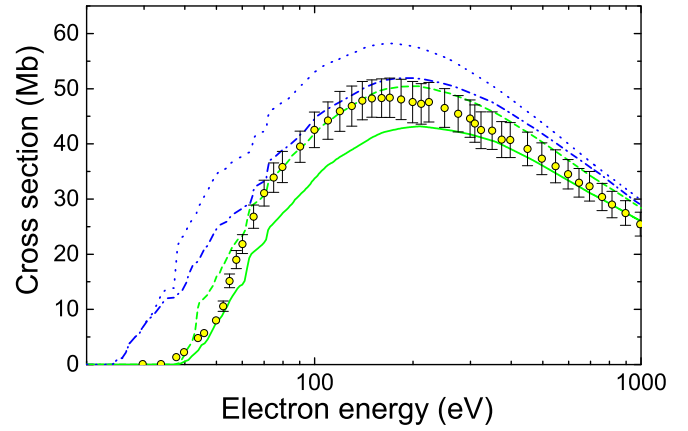


FIG. 9. Comparison of influence of CI effects to single-ionization cross sections for the levels of the  $3d^44s$  configuration. Solid green line: scaled DW cross sections with CI for level with index 37 (Table I); dashed green line: scaled DW cross sections for level 37; dash-dotted blue line: scaled DW cross sections with CI for level 99; dotted blue line: scaled DW cross sections for level 99. Experiment: open circles with error bars [3]. Logarithmic scale is used for electron energies. For further details, see the main text.

#### IV. CONCLUSIONS

The single-ionization cross sections are studied for the levels of the  $\text{Fe}^{3+}$  ion. The DFS approach is used to investigate energy levels, radiative and Auger transition probabilities, as well as electron-impact excitation and ionization cross sections. The study included the levels of the ground and first-excited  $3d^44s$  configurations. The strongest EA channels for the ground configuration correspond to the excitations from the  $3p$  shell. However, the excitations from the  $3d$  shell of the  $3d^44s$  configuration dominate at the lower energies of the electrons. It is demonstrated that the LLDW single-configuration cross sections overestimate measurements in a wide range of electron energies.

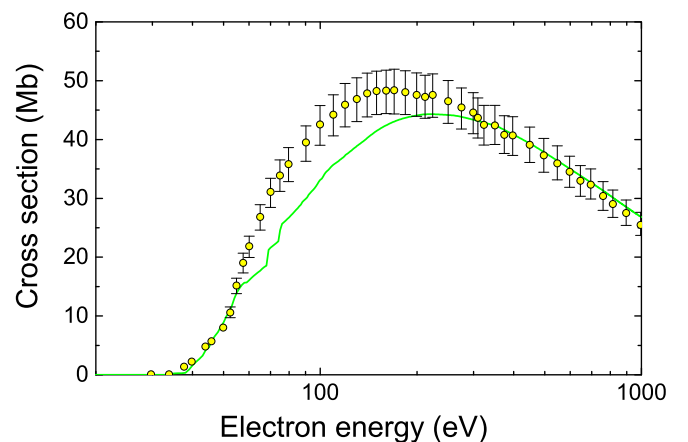


FIG. 10. Single-ionization cross sections obtained for the level with index 67 ( $J = 13/2$ ). Experiment: open circles with error bars [37]. Logarithmic scale is used for electron energies.

TABLE II. Maxwellian rate coefficients (in  $\text{m}^3 \text{s}^{-1}$ ) for levels of  $\text{Fe}^{3+}$ . Level indexes are taken from Table I. Temperatures ( $T_e$ ) are given in K. Note that  $a \pm b = a \times 10^{\pm b}$ .

$T_e$	Level index				
	0	36	37	67	90
8+4	4.796–18	3.098–17	1.853–17	3.810–17	2.001–16
2+5	7.674–16	1.462–15	9.632–16	1.295–15	2.839–15
4+5	4.835–15	6.767–15	4.437–15	5.283–15	8.435–15
8+5	1.359–14	1.678–14	1.108–14	1.263–14	1.695–14
2+6	2.743–14	3.171–14	2.151–14	2.418–14	2.889–14
4+6	3.481–14	3.942–14	2.753–14	3.062–14	3.491–14
8+6	3.801–14	4.261–14	3.100–14	3.362–14	3.684–14
2+7	3.627–14	4.037–14	2.710–14	2.809–14	2.937–14
4+7	2.916–14	3.234–14	1.706–14	1.732–14	1.773–14
8+7	1.805–14	1.998–14	8.335–15	8.371–15	8.480–15
2+8	6.769–15	7.486–15	2.589–15	2.583–15	2.601–15
4+8	2.756–15	3.047–15	9.820–16	9.777–16	9.822–16
8+8	1.048–15	1.158–15	3.597–16	3.578–16	3.590–16
2+9	2.770–16	3.062–16	9.297–17	9.241–17	9.267–17
4+9	9.941–17	1.099–16	3.311–17	3.290–17	3.299–17
8+9	3.541–17	3.914–17	1.175–17	1.167–17	1.170–17

The scaled DW cross sections in addition to correlation effects are studied to explain the measurements. The scaling of the DW cross sections for the levels of the ground and excited configuration leads to diminishing by  $\sim 40\%$  for the peak values. Negligible influence of correlation effects is obtained for the EA channels of the ground configuration. The correlation effects diminish the scaled DW cross sections by  $\sim 20\%$  for the lowest and the highest levels of the  $3d^4 4s$  configuration. Further studies are needed to determine the contribution of the resonant excitation double-autoionization process to single ionization in  $\text{Fe}^{3+}$ .

Finally, the current study provides compelling evidence that the available Maxwellian rate coefficients previously calculated using the DW cross sections for the ionization process in the  $\text{Fe}^{3+}$  ion are overestimated and their usage may lead to wrong predictions of charge state distribution in plasma.

#### ACKNOWLEDGMENT

Part of the computations was performed on resources at the High Performance Computing Center “HPC Saulėtekis” at the Vilnius University Faculty of Physics.

- [1] D. C. Griffin, C. Bottcher, and M. S. Pindzola, *Phys. Rev. A* **25**, 1374 (1982).
- [2] M. S. Pindzola, D. C. Griffin, C. Bottcher, S. M. Younger, and H. T. Hunter, *Nucl. Fusion* **27**, 21 (1987).
- [3] M. Stenke, U. Hartenfeller, K. Aichele *et al.*, *J. Phys. B: At. Mol. Opt. Phys.* **32**, 3641 (1999).
- [4] A. Müller, K. Tinschert, C. Achenbach, E. Salzborn, and R. Becker, *Nucl. Instr. Meth. B* **10-11**, 204 (1985).
- [5] M. S. Pindzola and S. D. Loch, *J. Phys. B: At. Mol. Opt. Phys.* **51**, 015202 (2018).
- [6] K. P. Dere, *Astron. Astrophys.* **466**, 771 (2007).
- [7] M. F. Gu, *Can. J. Phys.* **86**, 675 (2008).
- [8] V. Jonauskas, *Astron. Astrophys.* **620**, A188 (2018).
- [9] Y.-K. Kim, *Phys. Rev. A* **64**, 032713 (2001).
- [10] R. Karazija, *Introduction to the Theory of X-Ray and Electronic Spectra of Free Atoms* (Plenum Press, New York, 1996).
- [11] S. Kučas, V. Jonauskas, and R. Karazija, *Phys. Scr.* **55**, 667 (1997).
- [12] R. Karazija and S. Kučas, *J. Quant. Spectrosc. Radiat. Transfer* **129**, 131 (2013).
- [13] R. D. Cowan, *The Theory of Atomic Structure and Spectra* (University of California Press, Berkeley, 1981).
- [14] L. Radžiūtė, G. Gaigalas, D. Kato *et al.*, *J. Quantum Spectrosc. Radiat. Transfer* **152**, 94 (2015).
- [15] A. Kynienė, V. Jonauskas, S. Kučas, and R. Karazija, *R. Lithuan. J. Phys.* **48**, 219 (2008).
- [16] V. Jonauskas, R. Kisielius, A. Kynienė, S. Kučas and P. H. Norrington, *Phys. Rev. A* **81**, 012506 (2010).
- [17] V. Jonauskas, G. Gaigalas, and S. Kučas, *Data Nucl. Data Tables* **98**, 19 (2012).
- [18] V. Jonauskas, R. Karazija, and S. Kučas, *J. Phys. B: At. Mol. Opt. Phys.* **41**, 215005 (2008).
- [19] J. Palaudoux, P. Lablanquie, L. Andric *et al.*, *Phys. Rev. A* **82**, 043419 (2010).
- [20] V. Jonauskas, S. Kučas, and R. Karazija, *Phys. Rev. A* **84**, 053415 (2011).
- [21] S. Pakalka, S. Kučas, Š. Masys, A. Kynienė, A. Momkauskaitė, and V. Jonauskas, *Phys. Rev. A* **97**, 012708 (2018).
- [22] J. Koncevičiūtė, S. Kučas, Š. Masys, A. Kynienė and V. Jonauskas, *Phys. Rev. A* **97**, 012705 (2018).
- [23] J. Koncevičiūtė, S. Kučas, A. Kynienė, Š. Masys, and V. Jonauskas, *J. Phys. B: At. Mol. Opt. Phys.* **52**, 025203 (2019).
- [24] A. Kynienė, S. Kučas, Š. Masys and V. Jonauskas, *Astron. Astrophys.* **624**, A14 (2019).

- [25] A. Kramida, Yu. Ralchenko, J. Reader, and NIST ASD Team, NIST Atomic Spectra Database, ver. 5.6.1 (2019) (unpublished).
- [26] A. Kynienė, S. Pakalka, Š. Masys and V. Jonauskas, *J. Phys. B: At. Mol. Opt. Phys.* **49**, 185001 (2016).
- [27] A. Kynienė, Š. Masys and V. Jonauskas, *Phys. Rev. A* **91**, 062707 (2015).
- [28] A. Kynienė, G. Merkelis, A. Šukys, Š. Masys, S. Pakalka, R. Kisielius, and V. Jonauskas, *J. Phys. B: At. Mol. Opt. Phys.* **51**, 155202 (2018).
- [29] V. Jonauskas, A. Kynienė, G. Merkelis, G. Gaigalas, R. Kisielius, S. Kučas, Š. Masys, L. Radžiūtė, and P. Rynkun, *Phys. Rev. A* **91**, 012715 (2015).
- [30] A. Borovik, C. Brandau, J. Jacobi, S. Schippers, and A. Müller, *J. Phys. B: At. Mol. Opt. Phys.* **44**, 205205 (2011).
- [31] Y. K. Kim and M. E. Rudd, *Phys. Rev. A* **50**, 3954 (1994).
- [32] Y.-K. Kim and J.-P. Desclaux, *Phys. Rev. A* **66**, 012708 (2002).
- [33] D.-H. Kwon, Y.-J. Rhee, and Y.-K. Kim, *Int. J. Mass Spectrom.* **245**, 26 (2005).
- [34] D.-H. Kwon, Y.-J. Rhee, and Y.-K. Kim, *Int. J. Mass Spectrom.* **252**, 213 (2006).
- [35] V. Jonauskas, A. Pranciševičius, Š. Masys, and A. Kynienė, *Phys. Rev. A* **89**, 052714 (2014).
- [36] V. Jonauskas and Š. Masys, *J. Quantum Spectrosc. Radiat. Transfer* **229**, 11 (2019).
- [37] G. A. Alna'washi, N. B. Aryal, K. K. Baral, C. M. Thomas, and R. A. Phaneuf, *J. Phys. B: At. Mol. Opt. Phys.* **47**, 135203 (2014).